State Estimation Based Transmission Line Fault Locating with Sequence Distributed Parameter Models

Yu Liu, *Member, IEEE*, Yiran An, *Member, IEEE* and Boqi Xie, *Student Member, IEEE*

Abstract: This paper presents a novel phasor-domain dual-ended transmission line fault locating method enabled by sequence distributed parameter models and the state estimation algorithm. The method only requires fundamental frequency phasor measurements. Best implementation requires GPS synchronization at both terminals of the line. The method first models the transmission line with fault in sequence domain with distributed parameters, to accurately consider the effect of charging currents. Second, the state estimation algorithm is adopted to make full use of the redundancy in the fault locating problem and to cross check the estimated fault location. Numerical experiments demonstrate that the method has better accuracy than legacy fault locating methods, independent of fault types, locations and impedances.

Key words: Sequence distributed parameter models, fault locating, state estimation.

I Introduction

Transmission lines are very important devices inside power systems since they can transmit power over long distances and even interconnect different energy systems. Transmission line fault locating is an essential tool for utilities when a fault occurs inside a transmission line. It can reduce the time and effort spent searching for the fault, and therefore it will reduce the outage time and improve the power system reliability. Legacy transmission line fault locating approaches, including model based methods and measurement based methods, are introduced next.

A. Model based methods

These methods calculate the location of the fault based on the model of the transmission line with fault. For these methods, good accuracy of the fault locating results typically requires accurate parameters of the transmission line model. The most widely adopted methods are ***impedance based methods*** [1-3] (also known as phasor-domain model based methods). These methods use fundamental frequency current and voltage phasor measurements and compute the fault location by computing the impedance between the location of the fault and one terminal of the line. *Single-ended methods* only use voltage and current phasors at the local terminal of the line, without any requirements of communication channels from the remote terminal. However, the main disadvantage of single-ended methods is that the accuracy is greatly affected by fault impedances and source impedances [4]. To overcome these limitations [5], researchers also introduced *dual-ended methods*. These methods use phasor measurements from both terminals of the line and require communication channels from the remote terminal. They can be further categorized into methods that require GPS synchronized or non-synchronized measurements [6-7]. The disadvantages of existing phasor-domain methods are as follows: (a) for most of these methods, the modeling of transmission lines does not fully include distributed charging currents through the line during faults (neglecting shunt capacitances or considering lumped shunt capacitances only at terminals of the line); (b) these methods does not consider the redundancy inside the fault locating problem (the redundancy may potentially cross check the fault locating results and improve the fault locating accuracy). Moreover, researchers also proposed ***time-domain model based methods*** [8–10] other than phasor-domain model based methods. The main advantage of time-domain methods over phasor-domain methods is that time-domain methods do not filter out high frequency transients. Therefore, they are more accurate especially during system transients such as the period of time immediately after faults. However, these methods also have their own disadvantages. Most time-domain methods (for example in [8-9]) are based on Bergeron's method [11], where the present voltages and currents are expressed by voltages and currents a certain period of time ago. Note that this period of time is the time that the electromagnetic wave takes to travel from a selected terminal of the line to the location of the fault and could be extremely short. This causes the fact that the accuracy of the fault locating results highly depends on the sampling rate. Reference [10] presented a different time-domain method using dynamic state estimation, which does not require high sampling rates. However, the method is based on the multi-section π-equivalent transmission line model, which is an approximation of distributed parameter model.

B. Measurement based methods

These methods calculate the location of the fault based on the measurements only, and are hardly dependent on accurate parameters of transmission lines. The most widely used methods are ***traveling wave based methods*** [12-15], which

Yu Liu is with the School of Information Science and Technology (SIST), ShanghaiTech University, Shanghai, China, 201210 (e-mail: liuyu@shanghaitech.edu.cn).

Yiran An is with State Grid Shanghai Pudong Electric Power Supply Company, Shanghai, China, 200120 (email: anyiran_sgcc@163.com).

Boqi Xie is with the School of Electrical and Computer Engineering, Georgia Tech, Atlanta, GA, 30332 (email: bxie34@gatech.edu).

monitor the arrival time of traveling waves at one or both terminals of the line to estimate the location of the fault. *Single-ended methods* use arrival time difference of subsequent traveling waves at the local terminal to locate the fault [12-13], including Type A, C, E and F according to the way of generating the traveling waves. *Dual-ended methods* use arrival time difference between traveling waves at both terminals of the line to locate the fault [14-15], including Type B and D according to the way of synchronizing the two terminals. The disadvantages of traveling wave based methods are as follows: (a) the wavefront of traveling waves may not be reliably detected, since the intensity of traveling waves depends on the fault initiation time; and (b) even if the wavefronts are detected, the accuracy still highly depends on the sampling rate [16].

C. The proposed method

The state estimation algorithm has been widely adopted in power system to take advantage of redundant measurements [17-19]. In this paper, we propose a model based phasor-domain dual-ended method enabled by sequence distributed parameter modeling and the state estimation algorithm. It requires GPS synchronization at both terminals of the line. The proposed method solves the limitations of legacy phasor-domain methods from the following two aspects: (a) it accurately models distributed charging currents through the whole length of the line (sequence distributed parameter modeling); and (b) it makes full use of the redundancy inside the fault locating problem to further improve the fault locating accuracy (the state estimation algorithm). The rest of the paper is organized as follows. Section II reviews the theoretical backgrounds of transmission line modeling with sequence distributed parameters; section III describes the modeling procedure of transmission line with fault; section IV explains the state estimation algorithm procedure; section V demonstrates numerical experiment results; and section VI draws the conclusion.

II A Review: Transmission Line Modeling with Sequence Distributed Parameters

The three phase distributed parameter model of a transmission line is shown in Figure 1. The model consists of infinite number of sections where each section is a lumped parameter model of the infinitesimal length dx . Other definitions are: l is the total length of the transmission line; x is the distance between the left side of the line and the section dx shown in the figure; $\boldsymbol{i}(x,t)$, $\boldsymbol{v}(x,t)$, $\boldsymbol{i}(x+dx,t)$ and $\boldsymbol{v}(x+dx,t)$ are three phase currents and voltages at both terminals of the section dx; $\boldsymbol{i}_S(t)$, $\boldsymbol{v}_S(t)$, $\boldsymbol{i}_R(t)$ and $\boldsymbol{v}_R(t)$ are three phase currents and voltages at both terminals of the line; $\boldsymbol{R}_1$, $\boldsymbol{L}_1$, $\boldsymbol{G}_1$ and $\boldsymbol{C}_1$ are series resistance, series inductance, shunt conductance and shunt capacitance matrices per unit length (the corresponding mutual values are not depicted in the figure).

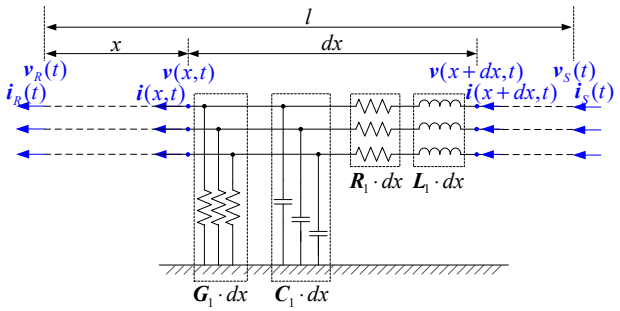

Figure 1. Distributed parameter transmission line model

The equations describing physical laws that this infinitesimal length line should obey are:

$$\begin{cases} \dfrac{\boldsymbol{v}(x+dx,t)-\boldsymbol{v}(x,t)}{dx}=\boldsymbol{R}_1\cdot\boldsymbol{i}(x+dx,t)+\boldsymbol{L}_1\dfrac{d\boldsymbol{i}(x+dx,t)}{dt} \\ \dfrac{\boldsymbol{i}(x+dx,t)-\boldsymbol{i}(x,t)}{dx}=\boldsymbol{G}_1\cdot\boldsymbol{v}(x,t)+\boldsymbol{C}_1\dfrac{d\boldsymbol{v}(x,t)}{dt} \\ \textit{Boundary conditions:} \quad \boldsymbol{i}(l,t)=\boldsymbol{i}_S(t),\ \boldsymbol{i}(0,t)=\boldsymbol{i}_R(t) \\ \qquad\qquad\qquad\qquad\quad \boldsymbol{v}(l,t)=\boldsymbol{v}_S(t),\ \boldsymbol{v}(0,t)=\boldsymbol{v}_R(t) \end{cases} \tag{1}$$

After taking the limit as $dx\to 0$ and substituting time domain waveforms (as functions of x and t) with fundamental frequency phasors (as a function of x only, at angular frequency ω), equation (1) becomes:

$$\begin{cases} \dfrac{d^2\tilde{\boldsymbol{V}}(x)}{dx^2}=(\boldsymbol{R}_1+j\omega\boldsymbol{L}_1)(\boldsymbol{G}_1+j\omega\boldsymbol{C}_1)\tilde{\boldsymbol{V}}(x) \\ \dfrac{d\tilde{\boldsymbol{V}}(x)}{dx}=(\boldsymbol{R}_1+j\omega\boldsymbol{L}_1)\tilde{\boldsymbol{I}}(x) \\ \textit{Boundary conditions:} \quad \tilde{\boldsymbol{I}}(l)=\tilde{\boldsymbol{I}}_S,\ \tilde{\boldsymbol{I}}(0)=\tilde{\boldsymbol{I}}_R \\ \qquad\qquad\qquad\qquad\quad \tilde{\boldsymbol{V}}(l)=\tilde{\boldsymbol{V}}_S,\ \tilde{\boldsymbol{V}}(0)=\tilde{\boldsymbol{V}}_R \end{cases} \tag{2}$$

where the capitalized letters with the superscript '~' are the phasor representations of the corresponding variable.

To solve equation (2), we adopt sequence transformation that converts the three phase distributed parameter model into positive, negative and zero sequence distributed parameter models. Therefore, equation (2) becomes three independent groups of equations, where $i=1,\ 2\ and\ 0$ correspond to equations representing positive, negative and zero sequence networks, respectively:

$$\begin{cases} \dfrac{d^2V_i(x)}{dx^2}=(r_i+j\omega l_i)(g_i+j\omega c_i)V_i(x) \\ \dfrac{dV_i(x)}{dx}=(r_i+j\omega l_i)I_i(x) \\ \textit{Boundary conditions:} \quad I_i(l)=I_{Si},\ I_i(0)=I_{Ri} \\ \qquad\qquad\qquad\qquad\quad V_i(l)=V_{Si},\ V_i(0)=V_{Ri} \end{cases} \tag{3}$$

The solution of equation (3) implies the following relationship among terminal currents and voltages:

$$\begin{bmatrix}\tilde{V}_{Ri}\\ \tilde{I}_{Ri}\end{bmatrix}=\begin{bmatrix}\cosh(\gamma_i\cdot l_f) & Z_i\sinh(\gamma_i\cdot l_f)\\ \dfrac{1}{Z_i}\sinh(\gamma_i\cdot l_f) & \cosh(\gamma_i\cdot l_f)\end{bmatrix}\begin{bmatrix}\tilde{V}_{Si}\\ \tilde{I}_{Si}\end{bmatrix} \tag{4}$$

where $Z_i = \sqrt{\dfrac{r_i + j\omega l_i}{g_i + j\omega c_i}}$ and $\gamma_i = \sqrt{(r_i + j\omega l_i)(g_i + j\omega c_i)}$.

Afterwards, three phase voltages and currents can be directly calculated from corresponding sequence values.

III Modeling of Transmission Lines with Fault

Here the way of modeling a transmission line with a single phase to neutral fault is introduced as an example, as shown in Figure 2 (for other types of faults, the way of modeling is quite similar). The model consists of three sequence models, where each sequence model consists of two separate line models using sequence distributed parameters according to equation (4). The connections among sequence networks are based on the type of fault.

Definitions of variables are as follows. $\tilde{I}_{Si}$, $\tilde{V}_{Si}$, $\tilde{I}_{Ri}$ and $\tilde{V}_{Ri}$ $(i = 1, 2, 0)$ are sequence currents and voltages at the both terminals of the line; $\tilde{I}_{fi}^{(1)}$ and $\tilde{I}_{fi}^{(2)}$ $(i = 1, 2, 0)$ are sequence fault currents flowing from the left side and the right side of the line at the location of the fault; $\tilde{V}_{fi}$ $(i = 1, 2, 0)$ are sequence voltages at the location of the fault; l is the total length of the line; l_f is the distance between the fault and the left terminal of the line; and Z_f is the fault impedance.

The equations describing physical laws that the circuit in Figure 2 should obey are:

$$\begin{cases}
\tilde{V}_{S1} = \cosh(\gamma_1 \cdot l_f)\tilde{V}_{f1} + Z_1 \sinh(\gamma_1 \cdot l_f)\tilde{I}_{f1}^{(1)} \\
\tilde{I}_{S1} = \dfrac{1}{Z_1}\sinh(\gamma_1 \cdot l_f)\tilde{V}_{f1} + \cosh(\gamma_1 \cdot l_f)\tilde{I}_{f1}^{(1)} \\
\tilde{V}_{R1} = \cosh\left[\gamma_1 (l - l_f)\right]\tilde{V}_{f1} + Z_1 \sinh\left[\gamma_1 (l - l_f)\right]\tilde{I}_{f1}^{(2)} \\
\tilde{I}_{R1} = \dfrac{1}{Z_1}\sinh\left[\gamma_1 (l - l_f)\right]\tilde{V}_{f1} + \cosh\left[\gamma_1 (l - l_f)\right]\tilde{I}_{f1}^{(2)} \\
\tilde{V}_{S2} = \cosh(\gamma_2 \cdot l_f)\tilde{V}_{f2} + Z_2 \sinh(\gamma_2 \cdot l_f)\tilde{I}_{f2}^{(1)} \\
\tilde{I}_{S2} = \dfrac{1}{Z_2}\sinh(\gamma_2 \cdot l_f)\tilde{V}_{f2} + \cosh(\gamma_2 \cdot l_f)\tilde{I}_{f2}^{(1)} \\
\tilde{V}_{R2} = \cosh\left[\gamma_2 (l - l_f)\right]\tilde{V}_{f2} + Z_2 \sinh\left[\gamma_2 (l - l_f)\right]\tilde{I}_{f2}^{(2)} \\
\tilde{I}_{R2} = \dfrac{1}{Z_2}\sinh\left[\gamma_2 (l - l_f)\right]\tilde{V}_{f2} + \cosh\left[\gamma_2 (l - l_f)\right]\tilde{I}_{f2}^{(2)} \\
\tilde{V}_{S0} = \cosh(\gamma_0 \cdot l_f)\tilde{V}_{f0} + Z_0 \sinh(\gamma_0 \cdot l_f)\tilde{I}_{f0}^{(1)} \\
\tilde{I}_{S0} = \dfrac{1}{Z_0}\sinh(\gamma_0 \cdot l_f)\tilde{V}_{f0} + \cosh(\gamma_0 \cdot l_f)\tilde{I}_{f0}^{(1)} \\
\tilde{V}_{R0} = \cosh\left[\gamma_0 (l - l_f)\right]\tilde{V}_{f0} + Z_0 \sinh\left[\gamma_0 (l - l_f)\right]\tilde{I}_{f0}^{(2)} \\
\tilde{I}_{R0} = \dfrac{1}{Z_0}\sinh\left[\gamma_0 (l - l_f)\right]\tilde{V}_{f0} + \cosh\left[\gamma_0 (l - l_f)\right]\tilde{I}_{f0}^{(2)} \\
0 = \tilde{I}_{f1}^{(1)} + \tilde{I}_{f1}^{(2)} - \tilde{I}_{f2}^{(1)} + \tilde{I}_{f2}^{(2)} \\
0 = \tilde{I}_{f1}^{(1)} + \tilde{I}_{f1}^{(2)} - \tilde{I}_{f0}^{(1)} + \tilde{I}_{f0}^{(2)}
\end{cases} \tag{5}$$

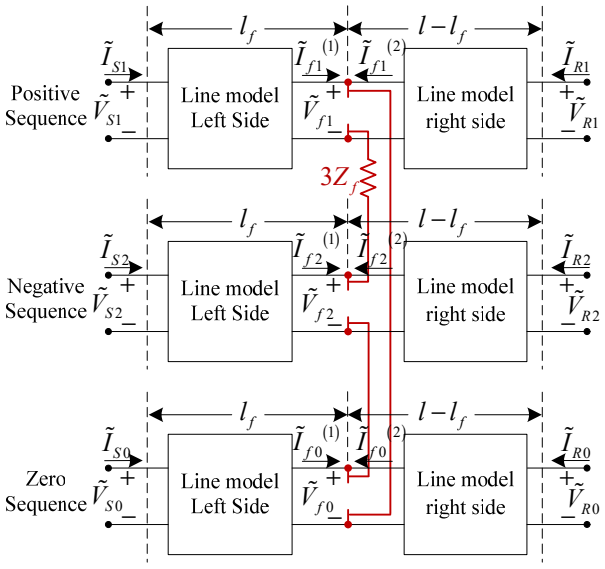

Figure 2. Modeling of a transmission line with single phase to neutral faults

Note that equation (5) is a complex number equation. It can be converted to a real number equation by separating the real and imaginary part for each row. For example, the first row of equation (5) becomes the following two rows after the conversion (full conversion results of equation (5) are not shown due to space limitations):

$$\begin{cases}
\tilde{V}_{S1,r} = \cosh(\alpha_1 l_f)\cos(\beta_1 l_f)V_{f1,r} - \sinh(\alpha_1 l_f)\sin(\beta_1 l_f)V_{f1,i} \\
\quad + Z_1 \sinh(\alpha_1 l_f)\cos(\beta_1 l_f)I_{f1,r}^{(1)} - Z_1 \cosh(\alpha_1 l_f)\sin(\beta l_f)I_{f1,i}^{(1)} \\
\tilde{V}_{S1,i} = \cosh(\alpha_1 l_f)\cos(\beta_1 l_f)V_{f1,i} + \sinh(\alpha_1 l_f)\sin(\beta_1 l_f)V_{f1,r} \\
\quad + Z_1 \sinh(\alpha_1 l_f)\cos(\beta_1 l_f)I_{f1,i}^{(1)} + Z_1 \cosh(\alpha_1 l_f)\sin(\beta_1 l_f)I_{f1,r}^{(1)}
\end{cases} \tag{6}$$

where the subscript 'r' and 'i' are the real and imaginary part of the corresponding phasor and $\gamma_1 = \alpha_1 + j\beta_1$.

This procedure generates the measurement model of the transmission line with fault, including the following two parts:

$$\boldsymbol{z}_{actual} = f(\boldsymbol{x}) \tag{7}$$

$$\boldsymbol{0} = g(\boldsymbol{x}) \tag{8}$$

where equation (7) corresponds to actual measurements of the model; equation (8) corresponds to constraints of the model; $\boldsymbol{z}_{actual}$ is the actual measurement vector; and $\boldsymbol{x}$ is the state vector. For this specific case, there exist 24 actual measurements, 4 constraints and 19 states (including the fault location l_f). Here we can observe the redundancy of the fault locating problem (degree of freedom = 24 + 4 – 19 = 9), which is not considered in legacy phasor-domain methods. The actual measurements and states are:

$$\begin{aligned}
\boldsymbol{z}_{actual} = \big[& V_{S1,r} \quad V_{S1,i} \quad I_{S1,r} \quad I_{S1,i} \quad V_{R1,r} \quad V_{R1,i} \quad I_{R1,r} \quad I_{R1,i} \\
& V_{S2,r} \quad V_{S2,i} \quad I_{S2,r} \quad I_{S2,i} \quad V_{R2,r} \quad V_{R2,i} \quad I_{R2,r} \quad I_{R2,i} \\
& V_{S0,r} \quad V_{S0,i} \quad I_{S0,r} \quad I_{S0,i} \quad V_{R0,r} \quad V_{R0,i} \quad I_{R0,r} \quad I_{R0,i} \big]^T
\end{aligned} \tag{9}$$

$$\boldsymbol{x}=\begin{bmatrix} V_{f1,r} & V_{f1,i} & I_{f1,r}^{(1)} & I_{f1,i}^{(1)} & I_{f1,r}^{(2)} & I_{f1,i}^{(2)} \\ V_{f2,r} & V_{f2,i} & I_{f2,r}^{(1)} & I_{f2,i}^{(1)} & I_{f2,r}^{(2)} & I_{f2,i}^{(2)} \\ V_{f0,r} & V_{f0,i} & I_{f0,r}^{(1)} & I_{f0,i}^{(1)} & I_{f0,r}^{(2)} & I_{f0,i}^{(2)} & l_f \end{bmatrix}^T \quad (10)$$

where the subscript 'r' and 'i' are the real and imaginary part of the corresponding phasor.

IV State Estimation Procedure

With the measurement model provided in equation (7), (8) and the corresponding measurements, we can directly compute the location of the fault l_f using the state estimation procedure. Here two algorithms are introduced next.

Algorithm 1: Constraint Weighted Least Square (CWLS)

The constraint overdetermined equations can be solved by the following optimization problem:

$$\begin{aligned} &Min \quad J=\left(f(\boldsymbol{x})-\boldsymbol{z}_{actual}\right)^T \boldsymbol{W}_{actual}\left(f(\boldsymbol{x})-\boldsymbol{z}_{actual}\right) \\ &Subject\ To \qquad \boldsymbol{0}=g(\boldsymbol{x}) \end{aligned} \quad (11)$$

where $\boldsymbol{W}_{actual}=diag\left\{\cdots,1/\sigma_i^2,\cdots\right\}$, and σ_i is the error standard deviation of the actual measurement *i,* and $(\cdot)^T$ means the transpose of $(\cdot)$.

To solve the above equation, we utilize the method of Lagrangian Multiplier with a new variable (Lagrangian Multiplier) $\boldsymbol{\lambda}$,

$$L=J+\boldsymbol{\lambda}^T g(\boldsymbol{x}) \quad (12)$$

The optimal solution of equation (11) has the following necessary condition:

$$\begin{cases} \partial L/\partial \boldsymbol{x}=\boldsymbol{0} \\ \partial L/\partial \boldsymbol{\lambda}=\boldsymbol{0} \end{cases} \quad (13)$$

The solution of equation (13) is provided with the following Newton's iterative algorithm until convergence:

$$\begin{bmatrix} \boldsymbol{x}^{\nu+1} \\ \boldsymbol{\lambda}^{\nu+1} \end{bmatrix}=\begin{bmatrix} \boldsymbol{x}^{\nu} \\ \boldsymbol{\lambda}^{\nu} \end{bmatrix}-\begin{bmatrix} \boldsymbol{F}^T\boldsymbol{W}_{actual}\boldsymbol{F} & \boldsymbol{G}^T \\ \boldsymbol{G} & \boldsymbol{0} \end{bmatrix}^{-1}\begin{bmatrix} \boldsymbol{F}^T\boldsymbol{W}\left(f(\boldsymbol{x}^{\nu})-\boldsymbol{z}_{actual}\right)+\boldsymbol{G}^T\boldsymbol{\lambda}^{\nu} \\ g(\boldsymbol{x}^{\nu}) \end{bmatrix} \quad (14)$$

where $\boldsymbol{F}=\partial f(\boldsymbol{x})/\partial \boldsymbol{x}\big|_{\boldsymbol{x}=\boldsymbol{x}^{\nu}}$ and $\boldsymbol{G}=\partial g(\boldsymbol{x})/\partial \boldsymbol{x}\big|_{\boldsymbol{x}=\boldsymbol{x}^{\nu}}$.

Algorithm 2: Unconstraint Weighted Least Square (UWLS)

To simplify the calculation procedure, the constraints shown in equation (8) can also be treated as 'virtual measurements' (with zero measurement values but with very small error standard deviations). In this way, the measurement model becomes:

$$z=\begin{bmatrix} \boldsymbol{z}_{actual} \\ \boldsymbol{0} \end{bmatrix}=\begin{bmatrix} f(\boldsymbol{x}) \\ g(\boldsymbol{x}) \end{bmatrix}=h(\boldsymbol{x}) \quad (15)$$

The overdetermined equation can be solved by the following optimization problem:

$$Min \quad J=\left(h(\boldsymbol{x})-\boldsymbol{z}\right)^T\boldsymbol{W}\left(h(\boldsymbol{x})-\boldsymbol{z}\right) \quad (16)$$

where $\boldsymbol{W}=diag\left\{\cdots,1/\sigma_i^2,\cdots\right\}$, and σ_i is the error standard deviation of measurement *i*.

The optimal solution of equation (16) has the following necessary condition:

$$\partial J/\partial \boldsymbol{x}=\boldsymbol{0} \quad (17)$$

The solution of equation (17) is provided with the following Newton's iterative algorithm until convergence:

$$\boldsymbol{x}^{\nu+1}=\boldsymbol{x}^{\nu}-\left(\boldsymbol{H}^T\boldsymbol{W}\boldsymbol{H}\right)^{-1}\boldsymbol{H}^T\boldsymbol{W}(h(\boldsymbol{x}^{\nu})-z) \quad (18)$$

where $\boldsymbol{H}=\partial h(\boldsymbol{x})/\partial \boldsymbol{x}\big|_{\boldsymbol{x}=\boldsymbol{x}^{\nu}}$.

Note that the results of algorithm 1 are slightly more accurate than algorithm 2. Since in this case the calculation burden is not increased much by switching from algorithm 2 to algorithm 1 (the most time consuming part is the matrix inverse: the matrix dimension is 12 by 12 for algorithm 1 and 10 by 10 for algorithm 2), algorithm 1 is used for all numerical studies in Section V.

The overall procedure of the proposed fault locating method is summarized in Figure 3.

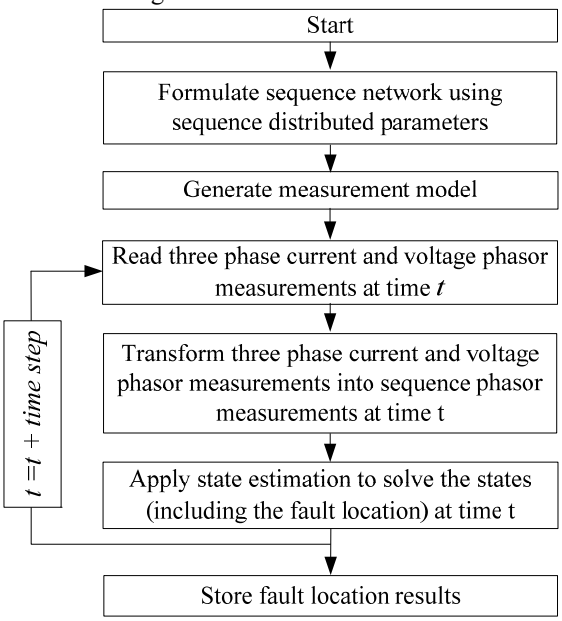

Figure 3. Flow chart of the proposed fault locating method

V Simulation Results

The example test system is a 60Hz, 500 kV transmission line system, as shown in Figure. 4 (the rest of the network is not shown). The transmission line of interest A1-A2 is a 4330 MVA, 135.22 mile line, with three phase voltage and current phasor measurements installed at both terminals of the line. We compare the performance of the legacy dual-ended impedance based method (referring to the IEEE standard in [12]) with our proposed method with different cases shown below. Due to space limitations, the fault locating results are provided only for single phase to neutral faults and three phase faults (the algorithm works equally well for other types of faults).

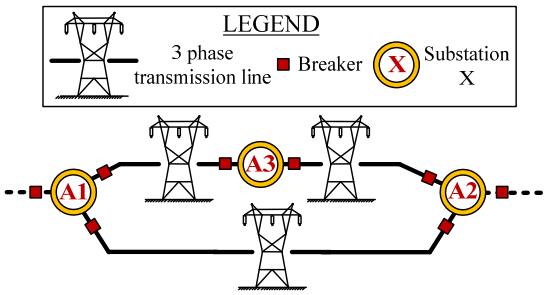

Figure. 4. 500 kV transmission line example test system

A. Case 1: bolted single phase to neutral faults

A 0.01 ohm phase A to neutral internal fault occurs at 30 miles from side A1 and at time 1.0 – 1.2 seconds. Figure 5 depicts the fault locating results of legacy dual-ended impedance based method and the proposed method. The fault locating results are 29.4785 miles for the legacy method and 29.7333 miles for the proposed method. By comparing the fault locating error of the proposed method (- 0.2667 miles) and the legacy method (- 0.5215 miles), we can observe that the proposed method is more accurate than the legacy method.

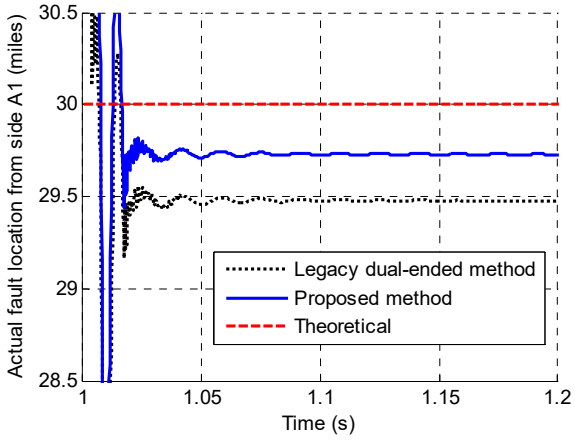

Figure 5. Fault locating results comparison, 0.01 ohm A-N fault, 1.0 – 1.2 s, 30 miles from side A1

To further examine the performance of the proposed method, 0.01 ohm phase A to neutral faults through the whole length of the line are tested. Figure 6 depicts the fault locating error of the legacy dual-ended impedance based method and the proposed method. The results suggest that the proposed method is more accurate than the legacy method.

B. Case 2: high impedance single phase to neutral faults

A 100 ohm phase A to neutral internal fault occurs at 30 miles from side A1 and at time 1.0 – 1.2 seconds. Figure 7 depicts the fault locating results of legacy dual-ended impedance based method and the proposed method. The fault locating results are 29.0411 miles for the legacy method and 29.4332 miles for the proposed method. By comparing the fault locating error of the proposed method (- 0.5668 miles) and the legacy method (- 0.9589 miles), we can observe that the proposed method is more accurate than the legacy method.

To further examine the performance of the proposed method, 100 ohm phase A to neutral faults through the whole length of the line are tested. Figure 8 depicts the fault locating error of the legacy dual-ended impedance based method and the proposed method. The results suggest that the proposed method is more accurate than the legacy method.

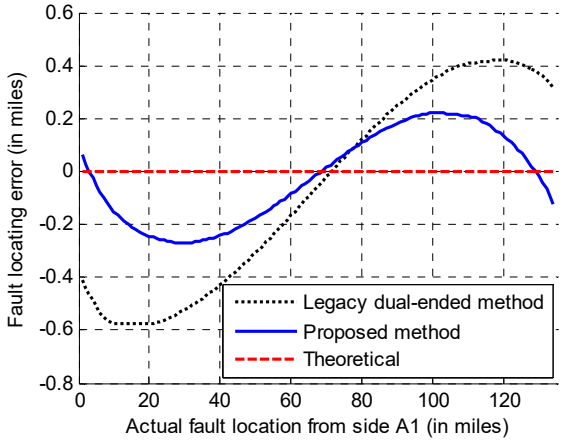

Figure 6. Fault locating results comparison, 0.01 ohm A-N faults, variable fault location

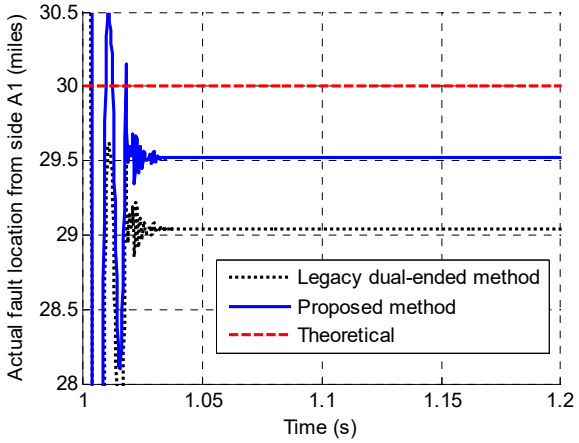

Figure 7. Fault locating results comparison, 100 ohm A-N fault, 1.0 – 1.2 s, 30 miles from side A1

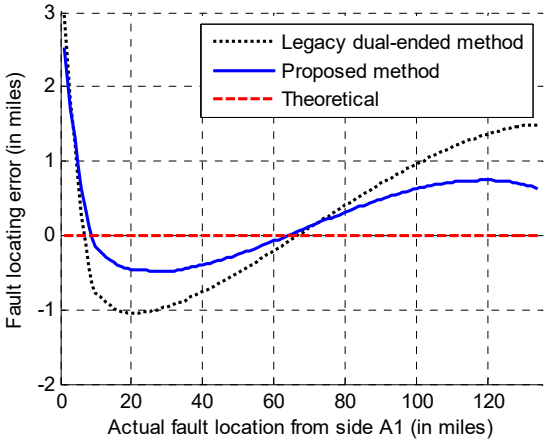

Figure 8. Fault locating results comparison, 100 ohm A-N faults, variable fault location

C. Case 3: bolted three phase faults

A 0.01 ohm three phase internal fault occurs at 30 miles from side A1 and at time 1.0 – 1.2 seconds. Figure 9 depicts the fault

locating results of legacy dual-ended impedance based method and the proposed method. The fault locating results are 29.0525 miles for the legacy method and 30.0553 miles for the proposed method. By comparing the fault locating error of the proposed method (0.0553 miles) and the legacy method (- 0.9475 miles), we can observe that the proposed method is more accurate than the legacy method.

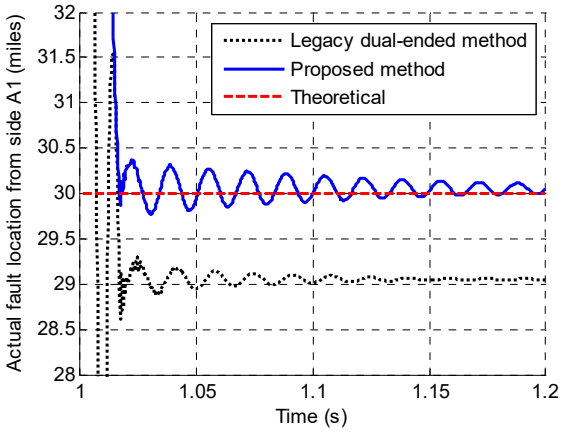

Figure 9. Fault locating results comparison, 0.01 ohm three phase fault, 1.0 – 1.2 s, 30 miles from side A1

To further examine the performance of the proposed method, 0.01 ohm three phase faults through the whole length of the line are tested. Figure 10 depicts the fault locating error of the legacy dual-ended impedance based method and the proposed method. The results suggest that the proposed method is more accurate than the legacy method.

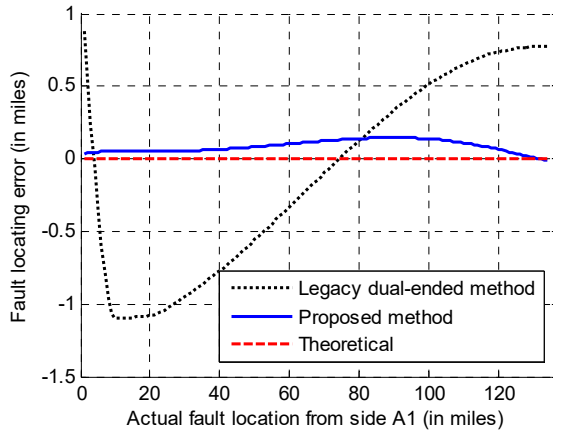

Figure 10. Fault locating results comparison, 0.01 ohm three faults, variable fault location

VI Conclusion

This paper proposed a state estimation based phasor-domain fault locating method with sequence distributed parameter models, to accurately find the location of the fault. First, the transmission line with fault is modeled using sequence distributed parameter models, which accurately consider distributed charging currents through the whole length of the line. Second, the method uses the state estimation procedure to make full use of the redundancy in the fault locating problem and to improve the fault locating accuracy. Compared with model based time-domain algorithms and measurement based algorithms, this method does not require high sampling rates and utilizes the fully distributed line model without π-equivalent approximations. Simulation results demonstrate that the proposed method has improved accuracy compared with the legacy dual-ended impedance based method and works for different fault types, locations and impedances. Future work directions include utilizing the three phase distributed parameter model without the assumption of symmetric parameters, and further test the performances in multi-terminal, inhomogeneous transmission lines.

References

[1] "SEL-351 Protection System Instruction Manual", Schweitzer Engineering Laboratories Inc., Pullman, WA, 2015.

[2] "GE D90^{Plus} Line Distance Protection System Instruction Manual", General Electric Multilin, Markham, Ontario, Canada, 2012.

[3] "Siemens SIPROTEC Line Differential Protection with Distance Protection 7SD5", Version 4.70, Siemens, Munich, Bavaria, Germany, 2011.

[4] Ha, H., Zhang, B., and Lv, Z.: 'A novel principle of single-ended fault location technique for EHV transmission lines', *IEEE Trans. Power Del.*, 2003, 18, (4), pp. 1147- 1151.

[5] Kawady, T., and Stenzel, J.: 'A practical fault location approach for double circuit transmission lines using single end data', *IEEE Trans. Power Del.*, 2003, 18, (4), pp. 1166–1173.

[6] Brahma, S. M., and Girgis, A. A.: 'Fault location on a transmission line using synchronized voltage measurements', *IEEE Trans. Power Del.*, 2004, 19, (4), pp. 1619-1622.

[7] Novosel, D., Hart, D.G., Udren, E., *et al*.: 'Unsynchronized two-terminal fault location estimation,' *IEEE Trans. Power Del.*, 1996, 11, (1), pp.130-138.

[8] Song, G., Suonan, J., Xu, Q., *et al*: "Parallel transmission lines fault location algorithm based on differential component net," *IEEE Trans. Power Del.*, 2005, 20, (4), pp. 2396-2406.

[9] Gopalakrishnan, A., Kezunovic, M., McKenna, S. M., *et al*:, "Fault location using the distributed parameter transmission line model," *IEEE Trans. Power Del.*, 2000, 15, (4), pp. 1169-1174.

[10] Liu, Y., Meliopoulos, A. P., Tan, Z., *et al*: "Dynamic State Estimation Based Fault Locating on Transmission Lines," *IET Generation Transmission Distribution*, in press.

[11] Dommel, H. W., "Digital Computer Solution of Electromagnetic Transients in Single-and Multiphase Networks, " *IEEE Trans. Power App. Syst.*, vol. PAS-88, no. 4, pp. 388-399, April 1969.

[12] IEEE Guide for Determining Fault Location on AC Transmission and Distribution Lines, IEEE Standard C37.114, 2014.

[13] Azizi, S., Sanaye-Pasand, M., Abedini, M., *et al*.: 'A traveling wave-based methodology for wide-area fault location in multiterminal DC systems,' *IEEE Trans. Power Del.*, 2014, 29, (6), pp. 2552–2560.

[14] Dewe, M. B., Sankar, S., and Arrillaga, J.: 'The application of satellite time references to HVDC fault location', *IEEE Trans. Power Del.*, 1993, 8, (3), pp. 1295–1302.

[15] Jafarian, P., and Sanaye-Pasand, M.: 'A traveling wave based protection technique using wavelet/PCA analysis', *IEEE Trans. Power Del.*, 2010, 25, (2), pp. 588–599.

[16] Suonan, J., Gao, S., and Song, G.: 'A Novel Fault-location Method for HVDC Transmission Lines', *IEEE Trans. Power Del.*, 2010 25, (2), pp. 1203–1209.

[17] Zhao, J., Zhang, G., Das, K., Korres, *et al*: "Power system real-time monitoring by using pmu based robust state estimation method," *IEEE Transactions on Smart Grid*, vol. 7, no. 1, pp. 300-309, Jan 2016.

[18] Meliopoulos, A. P., Cokkinides, G. J., Myrda, P., *et al*: 'Dynamic state estimation based protection: status and promise', *IEEE Trans. Power Del.*, 2017, 32, (1), pp. 320-330.

[19] Liu, Y., Meliopoulos, A. P., Fan, R., *et al*: 'Dynamic state estimation based protection on series compensated transmission lines', *IEEE Trans. Power Del.*, in press.